Fermi National Accelerator Laboratory

FERMILAB-Pub-93/191

Longitudinal Bunched-beam Instabilities Going Nonlinear: Emittance Growth, Beam Splitting and Turbulence

A. Gerasimov

Fermi National Accelerator Laboratory
P.O. Box 500, Batavia, Illinois 60510

July 1993

Submitted to *Physical Review E*

Operated by Universities Research Association Inc. under Contract No. DE-AC02-76CHO3000 with the United States Department of Energy

Disclaimer

Longitudinal bunched-beam instabilities going nonlinear: emittance growth, beam splitting and turbulence.

A.Gerasimov

Fermi National Accelerator Laboratory*
P.O.Box 500, Batavia, IL 60505, USA

July 14, 1993

Abstract

Numerical results of the nolinear evolution of longitudunal instabilities of bunched beams are presented. An argument is made for a rescaling of multi-bunch dynamics to a single-bunch case for the case of a narrow-band impedance exciting a single coupled-bunch mode. Saturation effects due to the decoherence caused by tune spread are categorized according to the magnitude and type of impedances. The new phenomenon of non-saturating instability (beam splitting) is described. Slow decay of instabilities after saturation with random-like bunch centroid oscillations ("beam turbulence") is observed and discussed.

1 Introduction

Coherent instabilities of beams in high-energy accelerators due to the interaction with self-induced wakefields were studied extensively over the last decades within the framework of the linearized Vlasov equation. In this approach, one solves for the complex-frequency of the small perturbations of the beam density. However, when dealing with an unstable situation,

*Operated by the Universities Research Association, Inc. under contract with the U.S.Dept. of Energy.

the method applies only to the very early stages of the instability development and is therefore of limited value. Furthermore, the practical issue of emittance growth due to an instability can not be clarified in the linear analysis.

The later, nonlinear stages of longitudinal instability evolution for a coasting beam were studied by a few authors /1-3/. Some numerical simulation studies were carried out for the bunched beam, but with the emphasis on a comparison with the linear theory and the thresholds of instabilities /4/. Numerical simulation results /1/ indicated that the longitudinal instabilities of a coasting beam always saturate and eventually decay due to the effect of decoherence. A theory of this phenomenon, predicting the energy spread blowup was developed in Refs./2/ and /3/.

In the present paper, we undertake a numerical simulation study of the late-stage, nonlinear development of longitudinal instabilities of bunched beams. Some phenomena observed are quite unusual for the accelerator physics domain and an effort is made to establish a qualitative connection with some esoteric concepts of plasma physics. This may allow a full theoretical description in the future.

The simulation is carried out for the simplest model which allows for the effects of nonlinear saturation of an instability due to the tune spread in the beam. This model consists of a single bunch interacting with a purely dipole-mode wakefield force (long wavelength/ low frequency impedance in the classification of Ref./5/). We present a theoretical argument that such a single-bunch model also describes the dynamics of a multi-bunch system when the impedance is narrow-band and peaked near a single revolution harmonic.

One of the major findings of our study is that the stabilizing effect of the tune spread depends very sensitively on the sign of the coherent frequency shift which is determined by the imaginary part of the effective impedance. When the coherent frequency is shifted from the synchrotron tune in the direction opposite to that of the incoherent tune spread (which is always negative for the sinusoidal RF potential), the instability can not be fully saturated by the decoherence due to the tune spread. One can observe instead that either the whole beam or a part of it that splits off the core oscillates with increasing amplitude without decohering. This beam splitting phenomenon is interpreted as the trapping of particles in the separatrices of self-excited nonlinear resonances, similar to the BGK modes in plasma physics.

Simulation results on emittance growth are presented from the perspec-

tive of an "overshoot" description. A simple scaling law for emittance growth with the centroid oscillation amplitude is derived for the case of a small synchrotron tune spread.

Late stages of instability development demonstrate a slow decay. The oscillations in this regime become random-like and the emittance continues growing. This behaviour is interpreted as a self-sustained "beam turbulence".

The plan of the paper is as follows: In Section 2, we present some theoretical cosiderations regarding the applicability of the model and the scaling of time evolution of observables with the tune spread and impedances. In section 3, we present the results of numerical simulations. Discussion and conclusions are given in Section 4.

2 Theoretical considerations.

2.1 The model.

We study the model of the longitudinal dynamics of a bunch interacting with a localized wakefield that is represented by the equations:

$$\begin{aligned} \ddot{x_i} + \omega_s^2 x_i - \lambda x_i^3 &= \sqrt{\frac{\epsilon}{N}} q \delta_{2\pi}(t) \\ \ddot{q} + \alpha \dot{q} + \omega_c^2 q &= \sqrt{\epsilon N}\, \bar{x} \delta_{2\pi}(t) \end{aligned} \tag{1}$$

where time is normalized to make the revolution frequency $\omega_0 = 1$, the quantity x_i is the coordinate of the i-th particle of a beam that consists of N particles, $\bar{x}$ is the coordinate of the centre of gravity of the beam $\bar{x} = \frac{1}{N}\sum_{i=1}^{N} x_i$, and q is the coordinate of a damped oscillator, coupled to the beam. The oscillator represents the amplitude of an effective single-mode impedance (see below). The interaction is periodic in time and instanteneous ($\delta_{2\pi}$ is a 2π-periodic δ-function). The parameter ϵ measures the strength of the interaction in the continuous limit $N \to \infty$ and is related to the conventional notations /5/ as $\epsilon = 2\pi e \frac{\omega_0 I_0}{E_0}$ (with e for electron charge, I_0 for the bunch current and E_0 for the particle energy). Frequencies ω_s and ω_c are respectively the synchrotron and resonant impedance frequencies. The constant $\lambda > 0$ measures the nonlinearity of the potential well for the beam particles and is always small in our study. This corresponds to the assumption that the beam occupies a small fraction of the RF bucket(s).

The model (1) can be derived based on the conventional considerations for the longitudinal motion of a single-bunch beam interacting with a single-

mode longitudinal wakefield, if the bunch length is assumed short relative to the wavelength of the wakefield (Long wavelength approximation in the analysis of Ref./5/). The detailed derivation is presented in Appendix A. The single-mode restriction is manifested in the pure harmonic (single-frequency) oscillations of the wakefield q. The condition of the long wavelength of the wakefield allows to keep only the lowest-order dipole-mode interaction.

Model (1) also applies to the multi-bunch case under certain conditions. In Appendix B we present the argument for the applicability of model (1) to the multi-bunch instability with an arbitrary impedance(including the many-modes case), that is peaked near a single revolution harmonic, and for the case of a weak interaction. The bandwidth of the impedance, $\Delta\omega_Z$ (the inverse of the characteristic decay time of the wakefield) has to satisfy the condition:

(i) restricted bandwidth

$$\delta\omega_s \ll \Delta\omega_Z \ll \omega_0 \tag{2}$$

where $\delta\omega_s$ is the tune spread in the bunches, $\delta\omega_s = \frac{3\lambda}{8\omega_s}\langle x^2\rangle$ and $\omega_0 = 1$ was left in its dimensinal form to emphasize the nature of the approximation. The other condition is that the interaction must be sufficiently weak:

(ii) weak interaction

$$\epsilon \ll \Delta\omega_Z \omega_s^2 \omega_c \tag{3}$$

This condition is often satisfied in cases of practical interest.

2.2 Stability analysis and scaling laws

Throughout this study we will assume that the condition *(i)* of restricted bandwidth is satisfied for our model (1) (with $\Delta\omega_Z = \alpha$). The dynamics then can be simplified to a (non-Hamiltonian) collective effective interaction of the particles in the beam as shown in Appendix B:

$$\ddot{x}_i + \omega_s^2 x_i - \lambda x_i^3 = \epsilon(-\tilde{Z}_i \bar{x} + \frac{\tilde{Z}_r}{\omega_s}\dot{\bar{x}}) \tag{4}$$

where the complex effective impedance $\tilde{Z} = \tilde{Z}_r + i\tilde{Z}_i$ is defined as $\tilde{Z} = Z(\omega_s)$, with the regular frequency-dependent impedance:

$$Z(\omega) = -\frac{i}{(2\pi)^2}\sum_n \frac{1}{\omega_c^2 + i\alpha(\omega+n) - (\omega+n)^2} \tag{5}$$

However, for the numerical simulation, we used the original model (1) as it can be cast in the form of discrete-time mapping, which allows a considerable economization of computer time.

The linear stability analysis of model (4) can be done by the conventional linearization of the Vlasov equation (see e.g. /5/). Since the nonlinearity λ is small, one can use the action-angle variables of the unperturbed linear oscillator, $I = \frac{1}{2\omega_s}(\dot{x}^2 + \omega_s^2 x^2)$, and $\theta = atan(\frac{\dot{x}}{\omega_s x})$ to obtain the dispersion relation for the complex coherent frequency ω of centroid oscillations $\bar{x} = ae^{i\omega t}$:

$$1 = i\epsilon\tilde{Z}\int_c \frac{dI\, I\frac{df_0}{dI}}{\omega^2 - (\omega_s^2 - \lambda' I)} \tag{6}$$

where $\lambda' = \frac{3\lambda}{4\omega_s}$, $f_0(I)$ is the unperturbed normalized density distribution and the integration is along the Landau contour. For a vanishingly small tune spread $\lambda \to 0$, and a weak interaction $|\epsilon\tilde{Z}| \ll \omega_s^2$, the complex coherent frequency shift $\Delta\omega_s = \omega - \omega_s$ is:

$$\Delta\omega_s = \frac{i\epsilon\tilde{Z}}{2\omega_s} \tag{7}$$

This defines both the growth rate $Im(\Delta\omega_s)$ and the (real) coherent frequency shift $Re(\Delta\omega_s)$.

It is often true under realistic conditions that both the coherent frequency shift $\Delta\omega_s$ and the incoherent tune spread $\delta\omega_s$ are small, so that one can use the approximation:

(iii) fast synchrotron oscillations

$$\begin{aligned} |\Delta\omega_s| &\ll \omega_s \\ |\delta\omega_s| &\ll \omega_s \end{aligned} \tag{8}$$

This approximation is used in the conventional linear stability analysis (see e.g. /5/). The synchrotron oscillations then are fast and can be averaged over. For the nonlinear evolution in system (4), the only relevant parameters left are $\delta\omega_s$, $Re(\Delta\omega_s)$ and $Im(\Delta\omega_s)$. Any one of these parameters defines the time scale, so that the "slow" evolution of coherent instability depends essentially on two dimensionless parameters:

$$\begin{aligned} C_r &= -\frac{Re(\Delta\omega_s)}{\delta\omega_s} \\ C_i &= -\frac{Im(\Delta\omega_s)}{\delta\omega_s} \end{aligned} \tag{9}$$

where the minus sign was inserted because the nonlinear tune shift is always negative, while the tune spread $\delta\omega_s$ is defined as a positive quantity. The stability border in the C_r, C_i plane for a gaussian distribution was obtained from our simulation results and is shown in Fig.1.

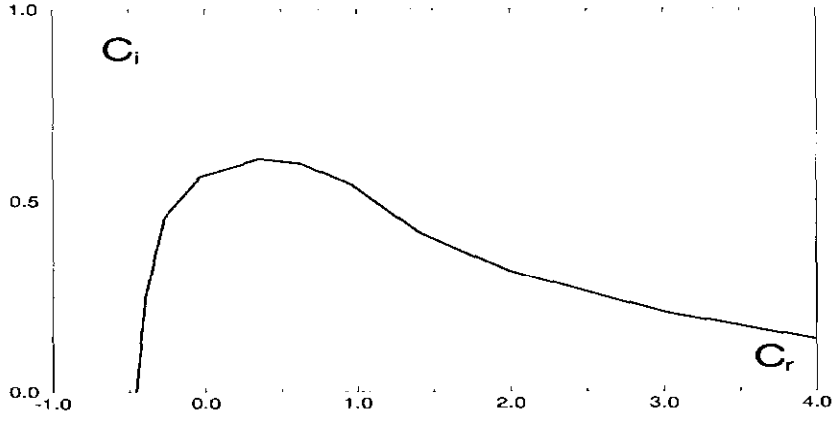

Fig.1 Stability border for the gaussian distribution $f_0 \sim e^{-I/(\omega_s\sigma)}$. The area under the curve is stable.

All quantities pertaining to the coherent instability evolution can be scaled in the form $y = y_0 f_y(\delta\omega_s t, C_r, C_i)$ where y_0 is the initial value and f_y is a dimensionless function of three dimensionless arguments. In the present study we will concentrate on interpreting and categorizing the scenarios of nonlinear evolution in terms of parameters C_r and C_i.

2.3 Energy balance and emittance growth.

The active part of the effective impedance $\tilde{Z}_r$ accounts for the energy loss (when $\tilde{Z}_r < 0$) or production (when $\tilde{Z}_r > 0$) in the system. This is clear for the case of a single particle $N = 1$, when $-\epsilon\frac{\tilde{Z}_r}{\omega_s}$ is the conventional damping decrement. For many particles, the energy balance is obtained from equation (4) in the form:

$$\frac{dW}{dt} = \frac{\epsilon N \tilde{Z}_r (\dot{\bar{x}})^2}{\omega_s} \tag{10}$$

where W is the total energy of the system, comprised of both the incoherent and interparticle interactions:

$$W = \sum_i \left(\frac{\dot{x_i}^2}{2} + \omega_s^2 \frac{x_i^2}{2} - \lambda \frac{x_i^4}{4} \right) + \frac{\epsilon N \tilde{Z}_i (\bar{x})^2}{2} \tag{11}$$

with $\bar{x} = 1/N \sum_i x_i$.

Under the condition *(iii)*, the parameters ϵ and λ are small, so that the frequency ω_s is a "fast" one. The motion of all particles then is separable into the slow and fast part as $x_i = \sqrt{\frac{2I_i}{\omega_s}} \cos(\omega_s t + \theta_i)$, with both action I_i and angle θ_i being slow variables. Averaging both parts of equation (10) over the fast oscillations and dropping the higher-order contributions from nonlinear and interparticle terms in W, one obtains the energy balance equation in the simplified form:

$$\frac{dW_0}{dt} = \epsilon N \omega_s \tilde{Z}_r A^2 \tag{12}$$

Here the unperturbed energy $W_0 = \sum_i \left(\frac{\dot{x_i}^2}{2} + \omega_s^2 \frac{x_i^2}{2} \right)$ and centroid oscillations amplitude $A = \sqrt{\frac{\dot{\bar{x}}^2}{\omega_s^2} + \bar{x}^2}$ (so that $\bar{x} = A \cos(\omega_s t + \varphi)$) are both slow functions of time.

In the slow-fast approximation, it is natural to define the emittance as the average over the fast oscillations, $\sigma = 1/N \left\langle \sum_i x_i^2 \right\rangle$, so that $\sigma = W_0 / N \omega_s^2$. Equation (12) defines then the rate of emittance growth and can be written as:

$$\frac{d\sigma}{dt} = \frac{A^2}{\tau_{gr}} \tag{13}$$

where τ_{gr} is the instability rise time in the absence of the tune spread $\tau_{gr} = \frac{1}{Im(\Delta\omega_s)}$. This simple scaling of emittance growth is a consequence of the fast synchrotron oscillations approximation *(iii)* and therefore applies only when the beam fills the small fraction of RF bucket.

3 Numerical simulation.

3.1 Scenarios of evolution: Strong Landau damping.

The evolution in model (1) is directly simulated by using many particles and implementing the single-turn mapping. In that mapping, the nonlinearity of

oscillations λ is treated perturbatively, i.e. the mapping for $x_i, \dot{x}_i$ between the δ-functional "kicks" is that of a linear oscillator with the frequency

$$\omega_s' = \omega_s - \frac{3\lambda}{8\omega_s^2}\left(\frac{\dot{x}_i^2}{2} + \omega_s^2\frac{x_i^2}{2}\right) \tag{14}$$

The number of particles N was taken to be large enough to reproduce the continuous limit and in cases close to the instability threshold was as high as $N = 10^5$.

We present the scenarios of instability evolution by dividing all cases in two categories: $C_r > 0$ (*Strong Landau damping*) and $C_r < 0$ (*Weak Landau damping*). The asymmetry of the stability border in C_r as seen in Fig.1 is indeed quite natural, since when the coherent tune is shifted outside of the nonlinear tune spread, no Landau damping is possible. The asymmetry of the linear stability diagram however is much less pronounced for other types of distributions like $f_0 \sim (1 - I/\omega_s\sigma)^2$ (see Ref./9/) so our terminology is more applicable to the properties of nonlinear saturation then to linear stability.

We first discuss the (*Strong Landau damping*) $C_r > 0$ category. Four characteristic examples of instability evolution in that category are presented in Figs.2-5. These examples are representative of four different scenarios that we loosely define by the relative strength of the instability (distance from threshold) and the type of impedance:

I) Strong instability $C_r \gg C_{rcr}$, $C_i \gg C_{icr}$
II) Weak instability $C_r \sim C_{rcr}$, $C_i \sim C_{icr}$

a) *Reactive impedance* $C_r > C_i$ (or $|Z_i| > |Z_r|$)
b) *Active impedance* $C_r < C_i$ (or $(|Z_i| < |Z_r|)$

The quantities $C_{rcr} = C_{rcr}(C_r/C_i)$, $C_{icr} = C_{icr}(C_r/C_i)$ are the critical (i.e.corresponding to the stability border) values for a given value of the ratio C_r/C_i. The quantity C_i is positive in all examples (negative C_i corresponds to the stable beam).

An example of scenario *Ia (Strong instability, Reactive impedance)* with parameters $C_r = 4.16$, $C_i = 1.65$ is shown in Fig.2. The time dependence of the centroid oscillations $\bar{x}(t)$ is plotted in Fig.2a. Emittance growth as a function of time $\sigma(t)$ is shown in Fig.2b. Samples of the corresponding phase space snapshots are shown in Fig.2c. Time is measured in number of turns (number of kicks in model (1)). The instability rise time in the absence of tune spread is $\tau_{gr} = 188.$ (turns).

The centroid oscillations in Fig.2a, as well as in all other cases to follow, presents itself as a fast-oscillating sinusoidal signal (with the synchrotron frequency) with a slowly changing envelope, since the parameters are chosen so as to satisfy the condition *(iii)*. The slow evolution in Fig.2a demonstrates 3 consecutive stages: 1) initial monotonic growth, 2) saturation at some rather high level (comparable to the size of the beam), and 3) slowly decaying oscillations of apparently random nature ("turbulence"). Transition from smooth "laminar" envelope to the "turbulent" behaviour occurs approximately at the saturation point. The monotonic growth of the envelope of oscillations until saturation is the characteristic feature of a *Strong instability* regime.

Emittance evolution is shown in Fig.2b. The maximum rate of emittance growth is occuring roughly at the saturation point. After saturation the emittance growth slows down considerably. We interpret it as a turbulent regime with slowly-decaying quasi-random oscillations.

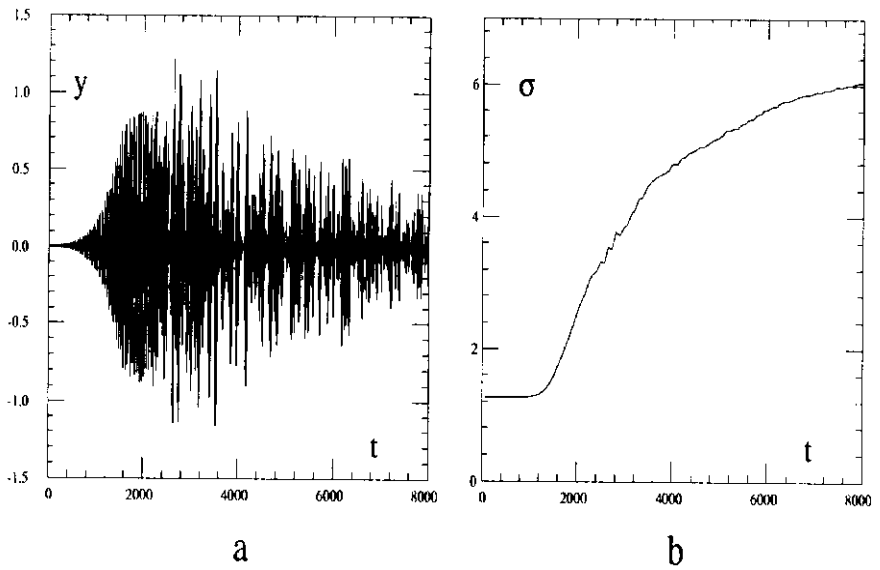

Fig.2. (**a**) Centroid oscillations $y = \bar{x}(t)$ and (**b**) Emittance growth $\sigma(t)$ for the case of (Strong instability, Reactive impedance) with $C_r = 4.16$, $C_i = 1.65$, and $\tau_{gr} = 188$..

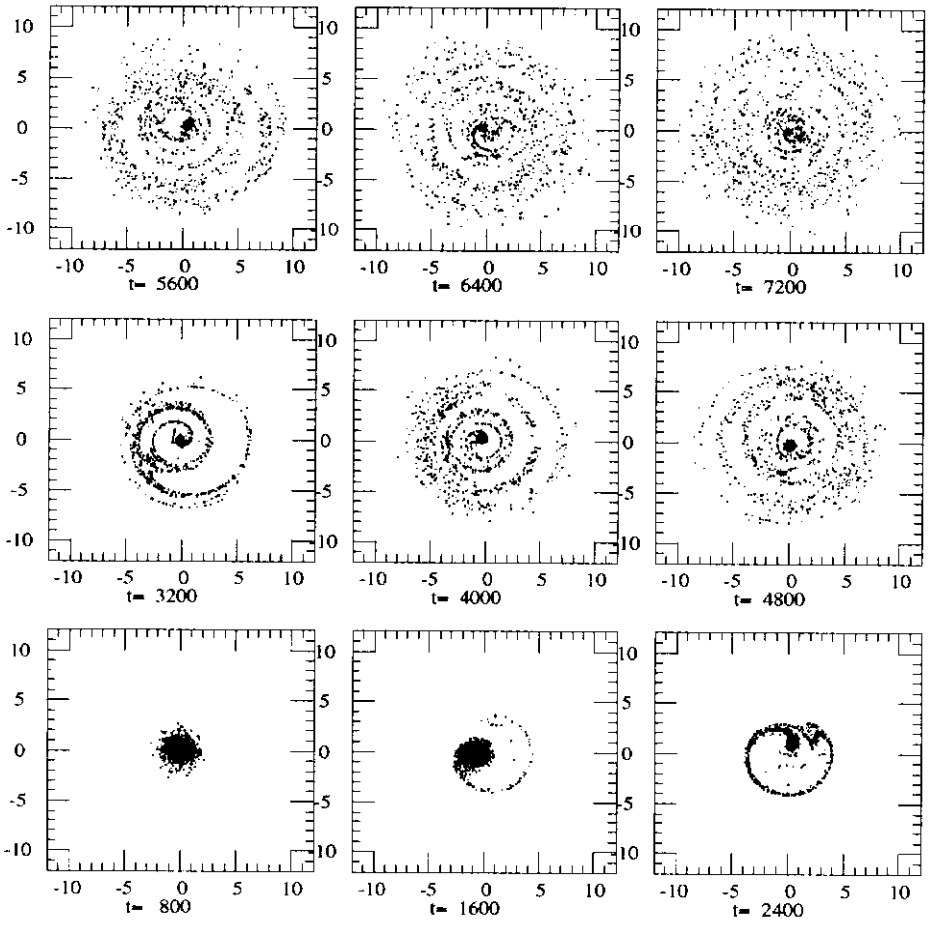

Fig.2c. Phase space snapshots for the parameters of Fig.2a and b.

In Fig.2c the phase space snapshots of the distribution are shown for 10 equidistant moments of time over the time span of evolution in Figs.2 a and b. These snapshots provide some insight into the nature of the processes leading to saturation and turbulence. One interesting property is that until saturation the bunch oscillates with increasing amplitude as a single entity without any visible effect of decoherence due to the tune spread. Closer to saturation, the bunch develops a thin "tail" of particles trailing behind it. After that, the bunch is losing particles to its tail, diminishing in size and returning back to the center of origin. The spiral-like tail of particle

density that the central bunch left behind is gradually decohering due to the phase-mixing. The remnants of the higher-density bunch near the center continues to maintain some small-scale motion, as the thin tail of that bunch is discernable for a long time.

An example of scenario **Ib** *(Strong instability, Active impedance)* for $C_r = 1.20$, $C_i = 4.56$is shown in Fig.3. The time dependence of centroid oscillations is presented in Fig.3a. The time scale is determined by $\tau_{gr} = 1221.$ (turns). The general pattern of evolution is similar to the previous case. The initial stage up to saturation is the monotonic growth of the oscillations. After saturation, the oscillations become random-like and decay slowly.

Emittance growth as a function of time is shown in Fig.3b. After saturation, the emittance growth is slowing down. A series of phase space snapshots are shown in Fig.3c. One feature of this series that is different from the previous case is that the particles that are located at larger radia (amplitude of oscillations) at the moment of saturation start moving toward increasing amplitudes in a sickle-like formation. This structure persists for some time, though particles are apparently being lost in the course of the radial motion, producing a sparce "tail" of density at large radia. We view this structure as a weak remnant of "trapped modes" that are observed for the *Weak Landau damping* regime $C_r < 0$ that is discussed in the next chapter.

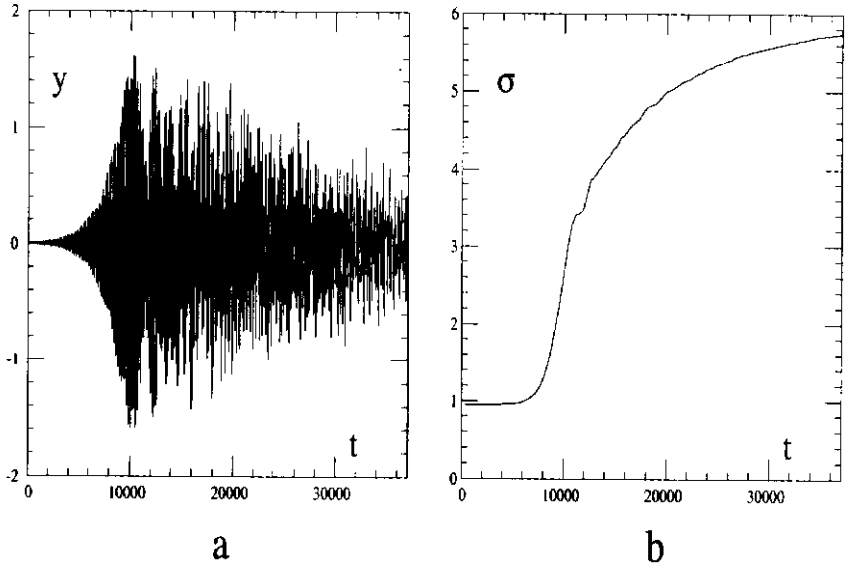

Fig.3 (**a**) Centroid oscillations $y = \bar{x}(t)$ and (**b**) Emittance growth $\sigma(t)$ for the case of (Strong instability, Active impedance) with $C_r = 1.20$, $C_i = 4.56$, and $\tau_{gr} = 1221$.

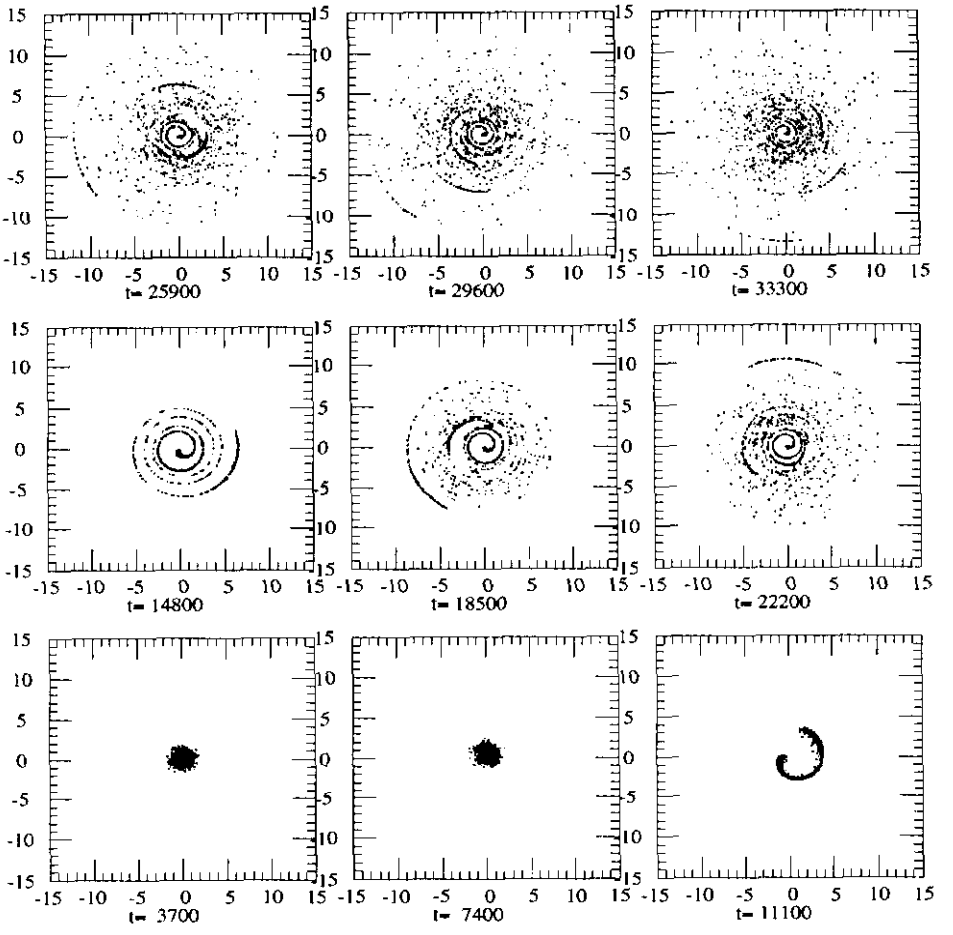

Fig.3c. Phase space snapshots for the parameters of Fig.3a and b.

An example of scenario ***IIa*** *(Weak instability, Reactive impedance)* for $C_r = 1.25$, $C_i = .49$ is shown in Fig.4. This case corresponds to about the same ratio C_r/C_i as for the case of Fig.2, and can represent then the same impedances but higher interaction strength ϵ (current in the ring).

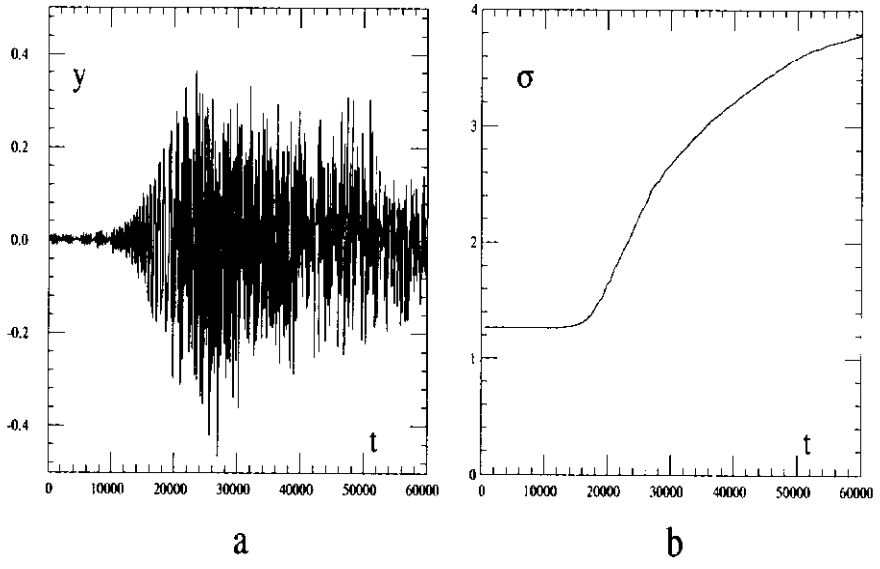

Fig.4. (**a**) Centroid oscillations $y = \bar{x}(t)$ and (**b**) Emittance growth $\sigma(t)$ for the case of (Weak instability, Reactive impedance) with $C_r = 1.25$, $C_i = .49$, and $\tau_{gr} = 315$.

The time dependence of the centroid motion is presented in Fig.4a. The time scale is defined by $\tau_{gr} = 315$. An important distinction from the previous cases is that the envelope of oscillations is not a monotonically growing function of time even before the saturation. The signature of the weak instability, as observed from this and other graphs, is threefold: 1) the initial growth rate of the instability is very slow, as one would expect from the linear theory, 2) the first maximum in the envelope of the oscillations occurs early before the saturation and is quite small. It is followed by several more maxima of increasing amplitude before the saturation, and 3) maximally attainable amplitudes of centroid oscillations are much smaller than in the case of a strong instability.

Emittance growth as a function of time is shown in Fig.4b. The saturation point on the emittance curve is less pronounced than in the case of a strong instability.

In Fig.4c the phase space snapshots of the distribution are shown for 10 equidistant moments of time over the time span of evolution in Figs.4a and

b. Most of the structure (radial and angular inhomogeneities) can be seen at $t = 18000$ and $t = 24000$, which are the moments of time close to when the saturation occurs.

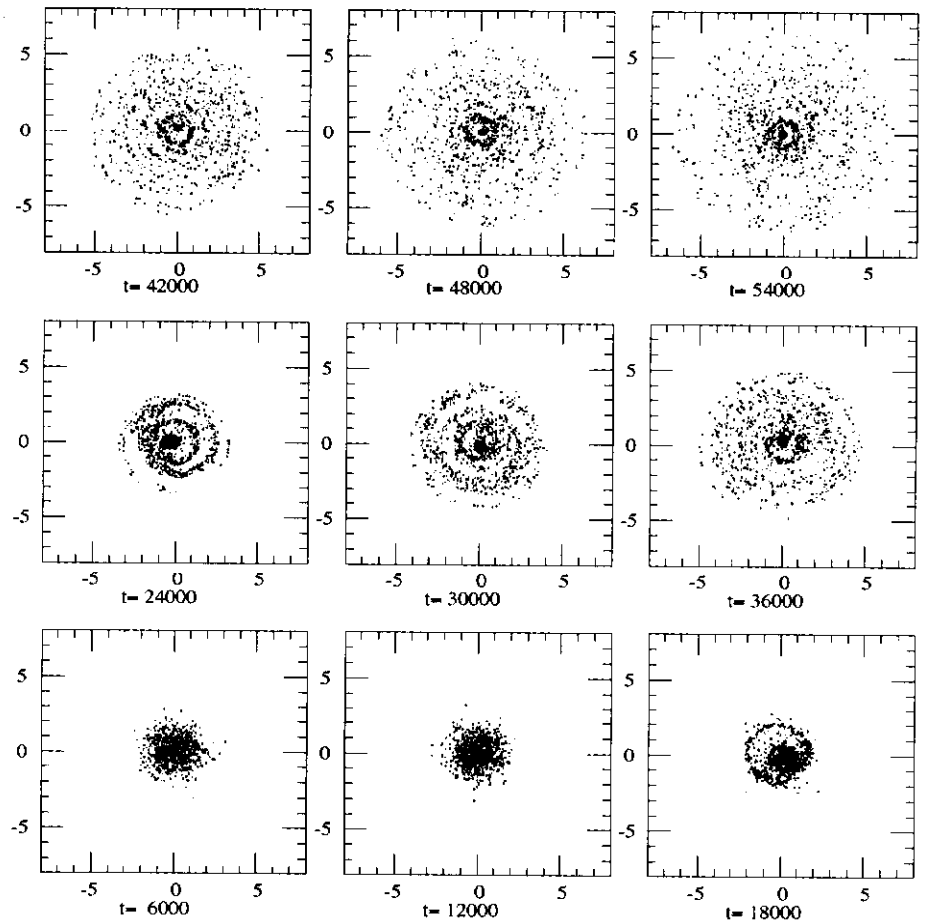

Fig.4c. Phase space snapshots for the parameters of Fig.4a and b.

An example of scenario *II*b' *(Weak instability, Active impedance)* for $C_r = .24$, $C_i = .89$ is shown in Fig.5.

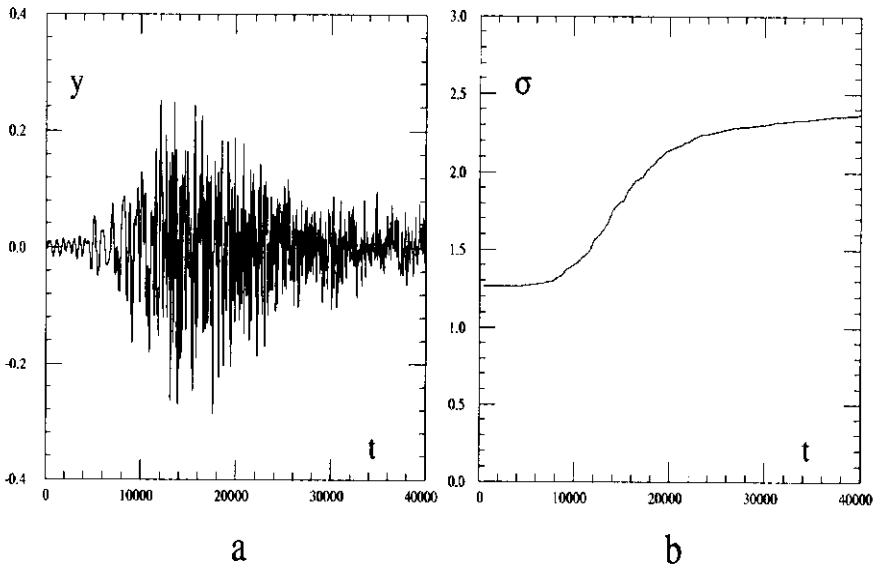

Fig.5. (**a**) Centroid oscillations $y = \bar{x}(t)$ and (**b**) Emittance growth $\sigma(t)$ for the case of (Weak instability, Active impedance) with $C_r = .24$, $C_i = .89$ and $\tau_{gr} = 175$.

The time dependence of the centroid motion is presented in Fig.5a. The time scale is defined by $\tau_{gr} = 175.$ (turns). All properties of the weak instability (1)-(3) are true in this case as well. An apparent randomization of oscillations is happening before saturation. The decay of these after the saturation is quite slow and does not appear to be determined by any relevant time constant of the system. Remember here that what looks like broadband oscillations in Fig.5a is still a relatively slowly modulated sinusoidal signal, since the time scale plotted is quite long.

Emittance growth as a function of time is shown in Fig.5b. Small undulations on the curve are real (not a computational artifact) and correspond to the local maxima in the envelope of oscillations of Fig.5a. As in previous examples, the emittance growth after saturation is slowing down but does not disappear altogether.

In Fig.5c the phase space snapshots of the distribution are shown for 10 equidistant moments of time over the time span of evolution in Fig.5a and b. Little structure can be discerned and one can only notice that azimuthal

and radial inhomogeneities of the density are quite irregular even before the saturation (which happens at about $t = 14000$).

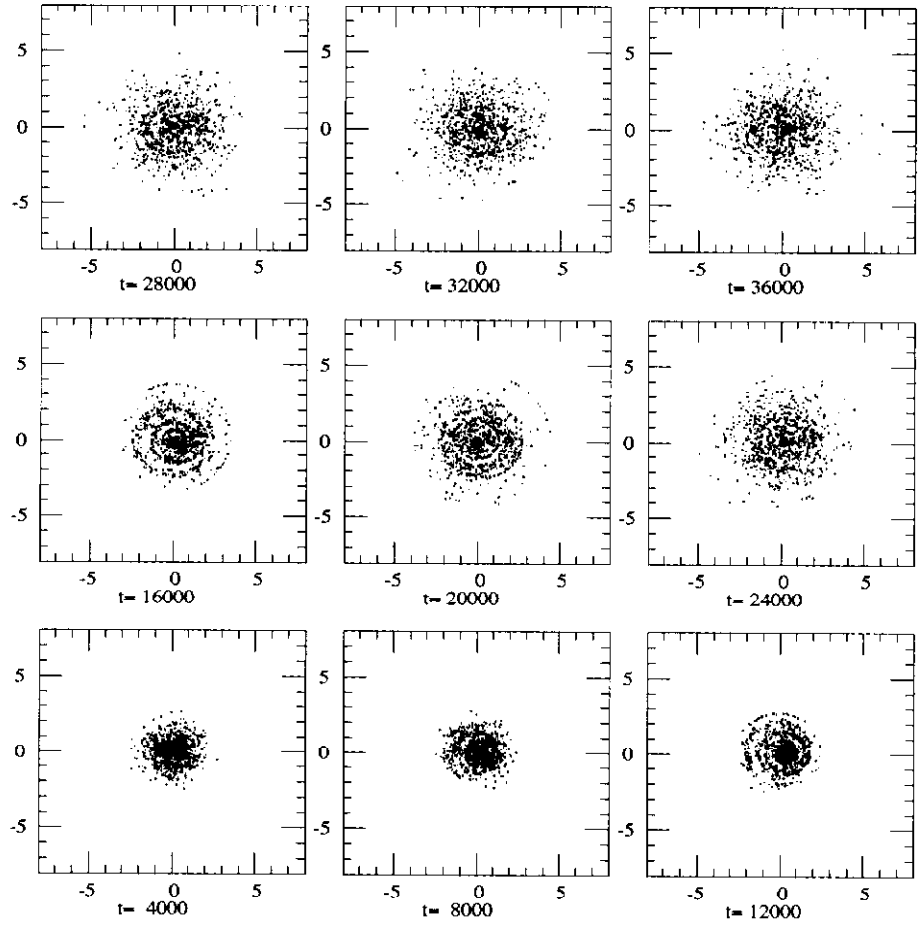

Fig.5c. Phase space snapshots for the parameters of Figs.5a and b.

3.2 Scenarios of evolution: Weak Landau damping.

In the case of *Weak Landau damping* $C_r < 0$ the scenarios of evolution are qualitatively different from the *Strong Landau damping* case $C_r > 0$. Two examples for different ratios C_r/C_i are presented in Figs.6 and 7.

An example of evolution of a relatively strong instability (not close to

the threshold) with the *Active type of impedance* (with parameters $C_r = -.64$, $C_i = 2.97$) is shown in Fig.6. Centroid oscillations and emittance as functions of time are shown in Figs.6a and b. The striking feature of these plots is that the instability does not saturate, as the centroid oscillations grow to the level of 7 times the initial size of the beam and continue growing. More insight into this behaviour is provided by the phase snapshot series of Fig.6c.

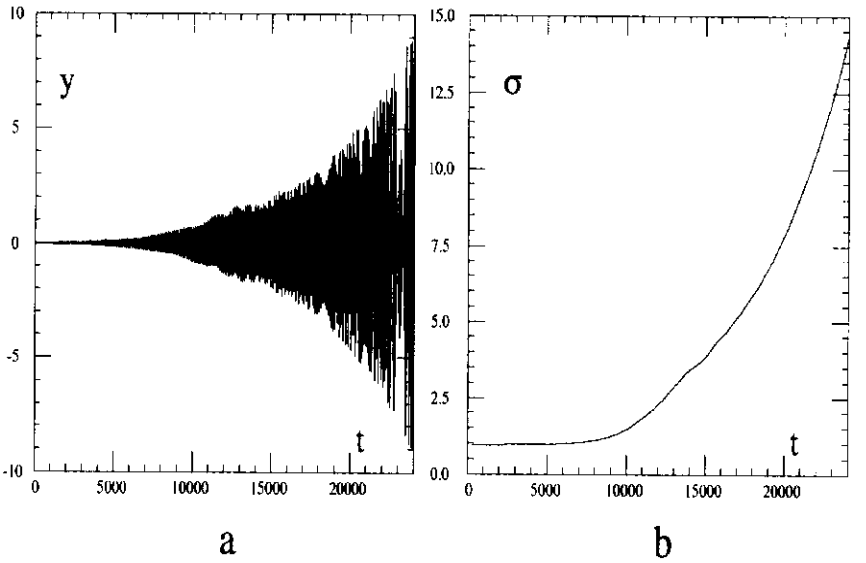

Fig.6. (**a**) Centroid oscillations $y = \bar{x}(t)$ and (**b**) Emittance growth $\sigma(t)$ for the case of (Weak instability, Active impedance) with $C_r = -.64$, $C_i = 2.96$ and $\tau_{gr} = 1880$.

Until the moment of time $t \sim 12000$ the bunch oscillates as a whole, while after that it decoheres into a spiral-like structure. After $t \sim 16000$, the outmost particles form a sickle-like "beamlet" that splits off the rest of the distribution and oscillates as a rigid entity with increasing amplitude. It is this nondecohering "beamlet" that causes unlimited growth of centroid oscillations and emittance in Figs.6 a and b.

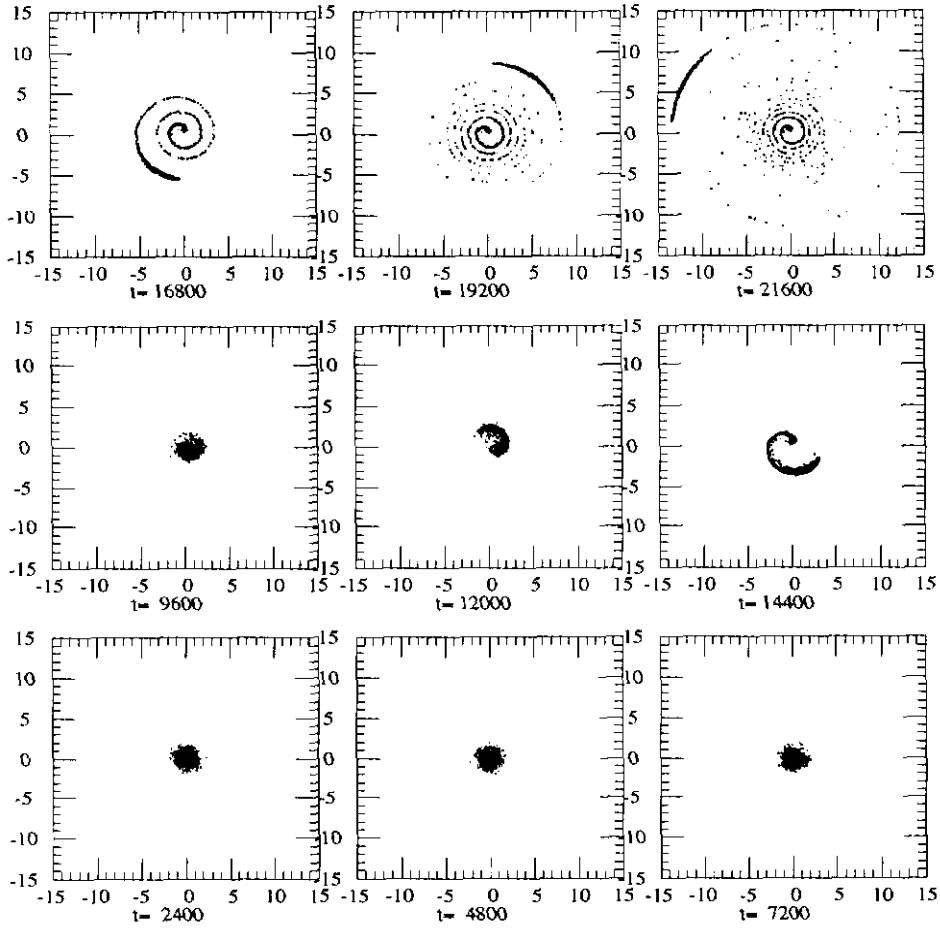

Fig.6c. Phase space snapshots for the parameters of Fig.6a and b.

An example of instability with even weaker Landau damping (larger negative C_r, *Reactive impedance*) with parameters $C_r = -2.89, C_i = 1.61$ is shown in Fig.7. Centroid oscillations and emittance time dependencies in Figs.7a and b again indicate an unlimited growth. The phase space snapshot series in Fig.7c shows that here nearly all particles are going into the nondecohering sickle-like formation, and just a tiny part of the bunch is left near the center.

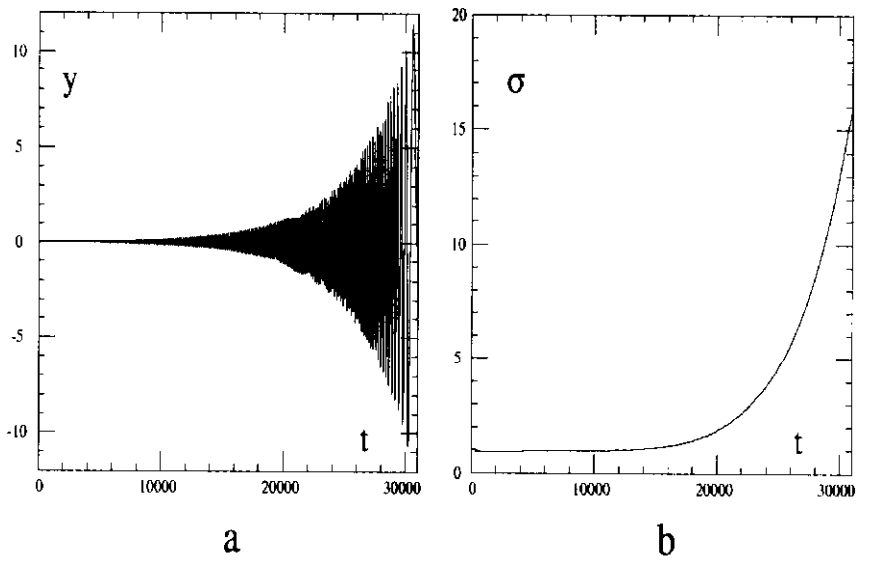

Fig.7. (**a**) Centroid oscillations $y = \bar{x}(t)$ and (**b**) Emittance growth $\sigma(t)$ for the case of (Weak instability, Active impedance) with $C_r = -2.89$, $C_i = 1.61$ and $\tau_{gr} = 3455$.

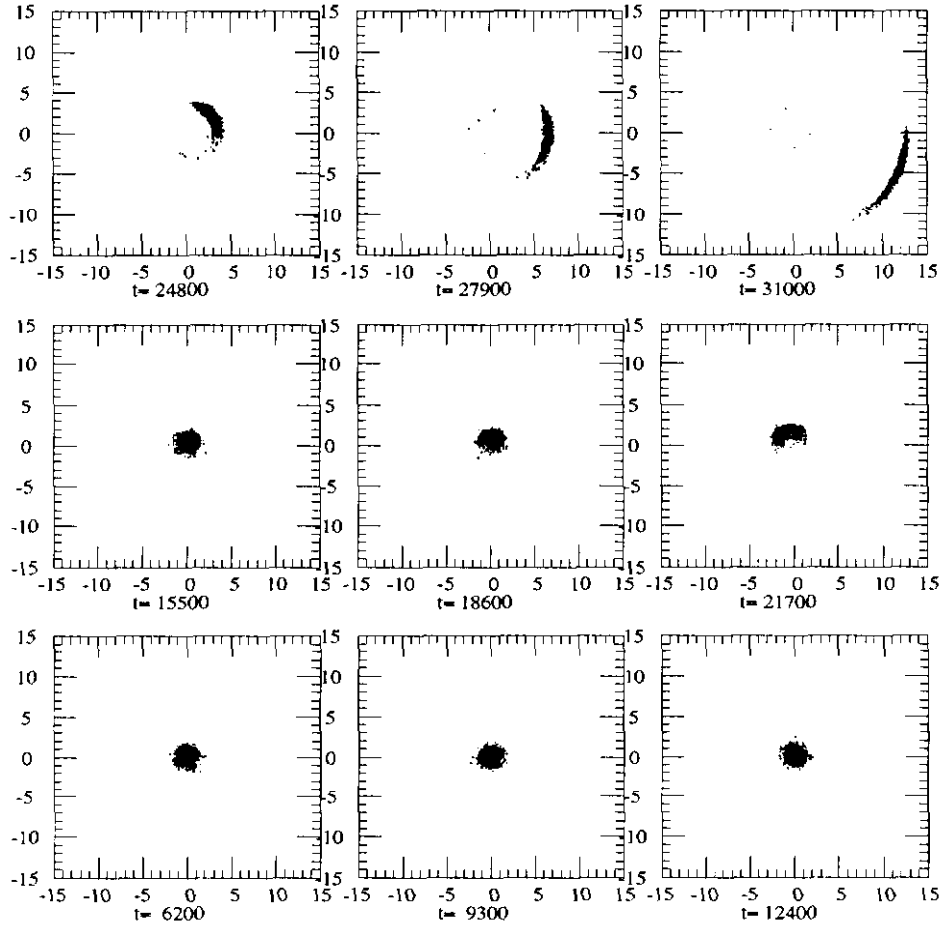

Fig.7c. Phase space snapshots for the parameters of Fig.7a and b.

We suggest the term "beam splitting" for the phenomenon of a nonsaturating instability through the formation of nondecohering "beamlets" (or whole beams). The border of the beam splitting region in the plane C_r, C_i was verified by many additional runs to be defined by the line $C_r = 0$ and the stability border of Fig.1. It was observed also that the border is a "soft" one, i.e. the percentage of particles trapped in the "beamlets" approaches zero when approaching the border. In some cases one can also see several "beamlets" successively splitting from the core of the distribution.

3.3 Emittance blowup and overshoot.

In the past, substantial effort was dedicated to study, both in theory and in simulation /1-3/, the energy spread blowup due to longitudinal instabilities of coasting beams. The main result of these studies was the identification and analysis of the overshoot phenomenon. This implies that the instability is always transient, and gradually dies away when the spread is blown up above the critical value. The term overshoot specifically alludes to the dependence of the final spread on the initial: the smaller is the latter, the larger the former.

In the bunched-beam model in the *Strong Landau damping* regime $C_r > 0$ the instability does not saturate and the concept of the overshoot does not apply. For *Weak Landau damping* $C_r < 0$ however the approach is justified and we studied the emittance blowup process from that perspective. The results of these simulations, when the initial emittances were changed while keeping the impedances Z_r, Z_i constant, are presented in Figs.8 and 9.

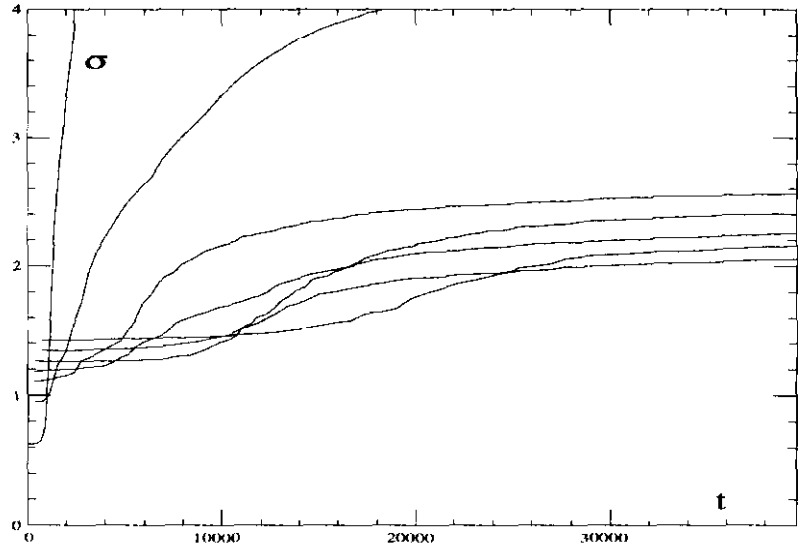

Fig.8. Emittance growth $\sigma(t)$ for different inital values $\sigma(0)$.
The impedances ratio is $C_i/C_r = 5.38$.

In Fig.8, the case of active impedance with the ratio $C_i/C_r = 5.38$

is shown. The basic pattern of emittance growth in this case follows the overshoot scenario. Slight deviations from this scenario though are noticable as well, as one can see some pairs of curves intersecting twice. Another feature is the sharp rise of emittance blowup for $\sigma(0) < 1$.. It is associated somehow with the transient sickle-like structures as seen in Fig.3c.

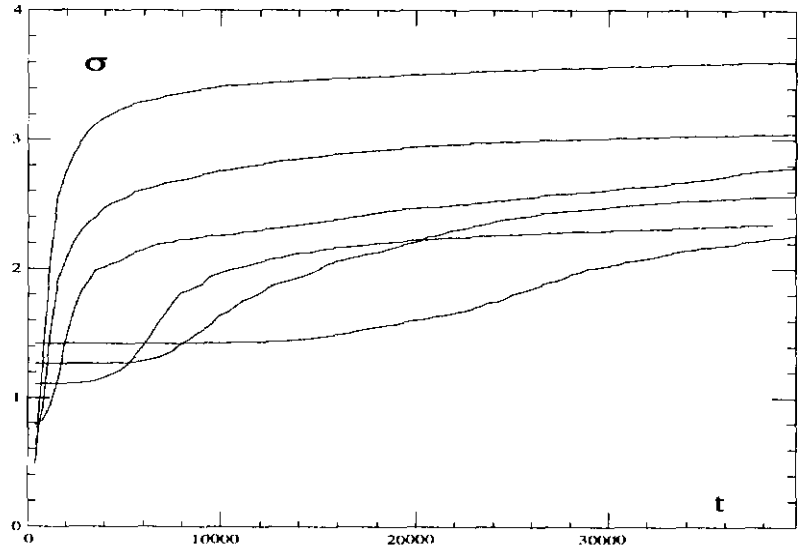

Fig.9. Emittance growth $\sigma(t)$ for different inital values $\sigma(0)$. The impedances ratio is $C_i/C_r = 1$.

In Fig.9, the rise of emittance blowup with the lowering of $\sigma(0)$ is more gradual then in Fig.8. One can again see some peculiarities in emittance growth near the instability threshold, with the curves intersecting twice. It can also be noticed that near the threshold the emittance does not always completely saturate, but rather continues some slow growth. We return to the discussion of this phenomenon in the next section.

3.4 Beam turbulence

Centroid oscillations after the saturation in *Strong Landau damping* regime $C_r > 0$ appeared to a certain degree random in all the examples that were given so far. To quantify this randomness, we took a series of power spectra

of relatively short sections of centroid oscillations $\bar{x}(t)$. The length of the series was chosen to cover the duration of the period up to and around the saturation. The centroid oscillations and emittance growth for this example are shown in Figs.10 a and b. The values of $C_r = 1.12$, $C_i = 1.12$ are not very close to the stability border (see Fig.1). In Fig.10a, one can see the distinct irregular outbursts of centroid oscillations after saturation that also produce small irregular steps in the curve $\sigma(t)$ in Fig.10b in accordance with the emittance growth scaling law (13).

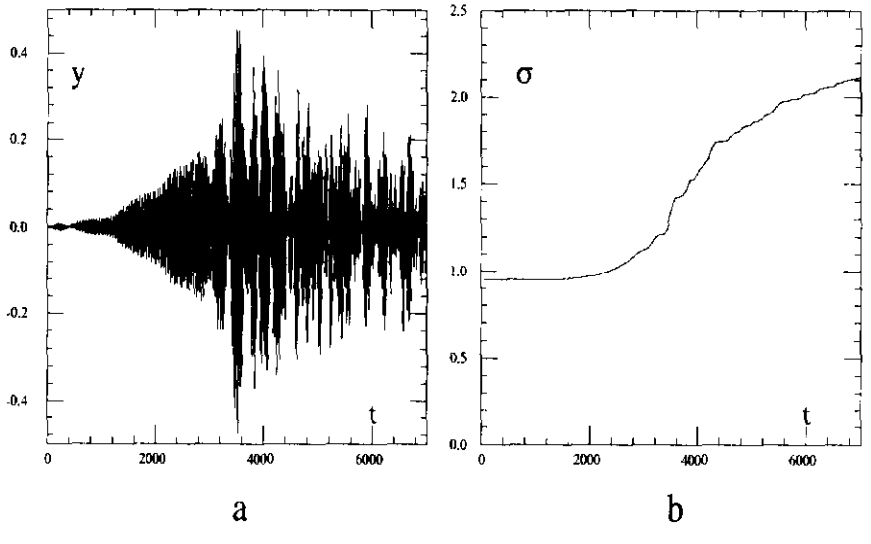

Fig.10. Beam turbulence: oscillation randomization after saturation. (**a**) Centroid oscillations $y = \bar{x}(t)$ and (**b**) Emittance growth $\sigma(t)$ for the case $C_r = 1.12$, $C_i = 1.12$ and $\tau_{gr} = 122$.

In Fig.10c we present the series of the power spectrum evolution for the sections of the signal $y(t)$ of Fig.10a. The whole period was divided in 10 sections, and time labels refer to the end of each section. Different plots were scaled vertically to have the same height of the peaks. Before the saturation at about $t = 3000$ the spectra are clearly single-peaked and quite narrow. After the saturation (the plot at $t = 3816$), the spectrum becomes broader several times and develops a multi-peaked structure. This proves our thesis of the randomization of oscillations, or the onset of turbulence, after the

saturation.

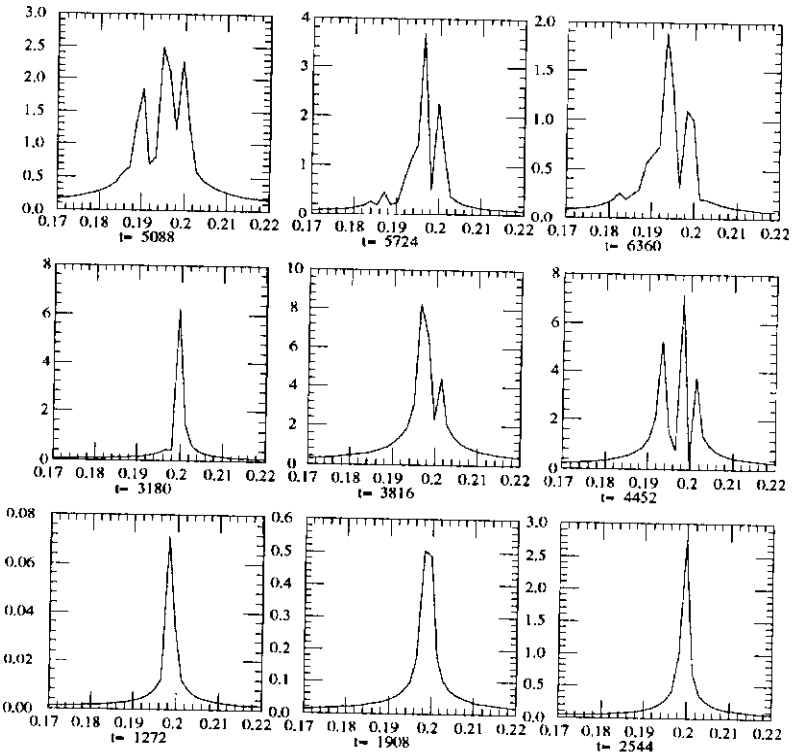

Fig.10c. Evolution of short-term power spectrum of centroid oscillations in Fig.10a. Synchrotron frequency is $\omega_s = .2$.

The question of the long-term behavior of the instability was touched upon in Section 3.3. It appeared from the data in that section that the instability, at least in some cases, does not completely decay after the saturation. Instead, one observes low-level quasirandom(turbulent) centroid oscillations that persist for a long time after the saturation and cause a slow emittance growth. One more example of a long-term evolution of this kind for the case of Fig.10a,b is given in Fig.10d. The sensitivity of the long-term turbulent emittance growth to the number of particles in the simulation is very high ($N = 3.10^5$ particles were required to reproduce the continuous limit in this case).

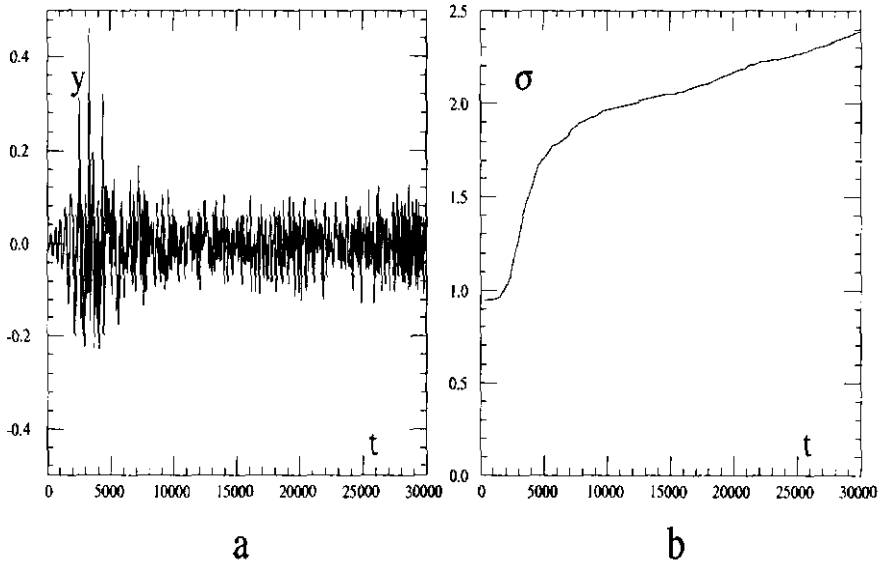

Fig.10d. Nondecaying low-level turbulence for the case of Fig.10a,b. (**a**) Centroid oscillations $y = \bar{x}(t)$ and (**b**) Emittance growth $\sigma(t)$ for the case $C_r = 1.12$, $C_i = 1.12$ and $\tau_{gr} = 122$.

The phase space plots after the saturation in all previous examples show only small azimuthal inhomogeneities that are hardly discernable by eye. That is the case as well for the tubulent stage of Fig.10. To provide more insight into the nature of the turbulence, we present in Fig.10e a few line density profiles for the case of Fig.10a,b. One can see that the turbulent regime corresponds to the presence of a short-wavelength low-apmplitude "microstructure" or "jitter" on top of a smooth density profile. This microstructure undergoes relatively fast (on the scale of the time span of Figs.10a-e) variations that appear to be random.

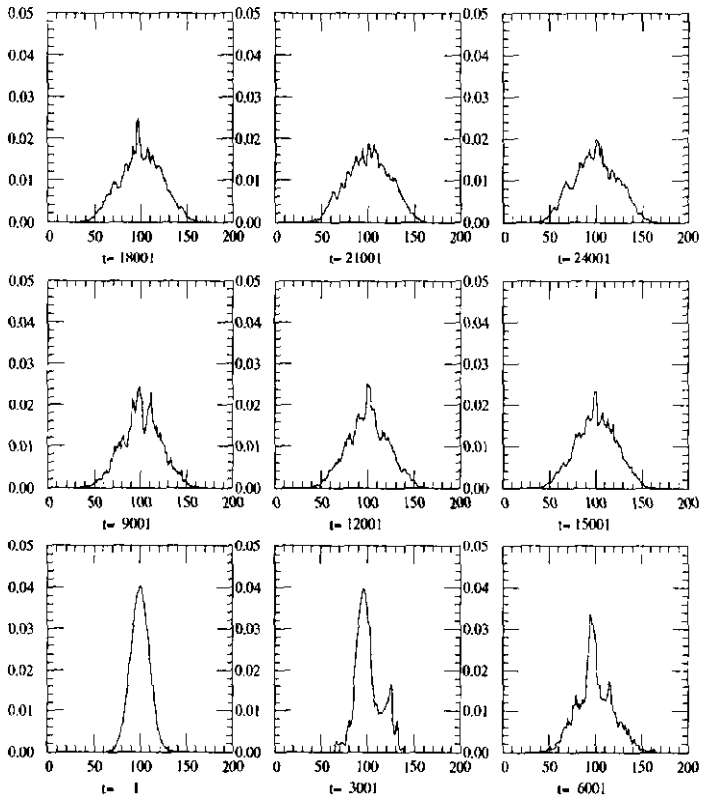

Fig.10e. Line density profiles evolution for the case of Fig.10a,b.

4 Discussion and conclusions.

The physics of the observed nonlinear phenomena of saturation, beam splitting and turbulence is far from being fully clarified by our numerical findings. This calls for a future study, and we would like to make a few suggestions in that direction.

The most striking of all nonlinear effects observed is the nonsaturating instability/beam splitting phenomenon that happens for *Weak Landau damping* regime $C_r < 0$. We suggest that this may be interpreted as the trapped-particle nonlinear modes, in extension of a similar concept of persistent nonlinear (BGK) waves in plasma physics (see, e.g. /6/). We expect by that analogy that in our system a group of particles can stay, under certain conditions, near the center of the self-driven nonlinear resonance.

The elongated shape of the "beamlets" in Figs.6c and 7c corraborates that interpretation, since that is what one would expect to see for a distribution of particles near the center of a narrow resonance.

The conceptual importance of the BGK modes in plasma physics stems from the fact that they present themselves as persistently oscillating states where no energy exchange between the particles and the wave is taking place. In our case, the energy is pumped into the system by the real part of the impedance (see equation (10)), and persistent steady-state oscillations are impossible. The trapped (BGK) modes for our system can be visualized as the states without any Landau damping, with the amplitude of a dipole oscillations increasing in time by taking the energy from the external source (which is eventually the RF system). The resonant frequency will change as well, while the particles stay inside the separatrix of the resonance as it moves towards larger radia. The difference with conventional BGK modes is in this (anti)dissipation in the system that causes the frequency sliding. Thus we suggest the term "sliding trapped (BGK) modes". A preliminary result is that these modes exist only for the *Weak Landau damping* regime $C_r < 0$, conforming with our observations of instability development scenarios. One can anticipate obtaining a theoretical description of beam splitting phenomenon on the basis of this approach.

Beam turbulence is another class of essentially nonlinear phenomena. Even after saturation when the emittance becomes large enough to make a beam stable for any smooth bell-shaped distribution, the small-scale "microstructure" of the density can persist in the beam for a long time, causing low-level centroid oscillations and slow emittance growth. This may be an issue of practical importance and requires a further study.

Emittance growth is related to the amplitude of the centroid oscillations through the convinient scaling law (13). The self-consistent theoretical prediction of how the oscillations will evolve is however very difficult. Some estimates of this kind were obtained in a quasilinear "overshoot" approach /7/ along the same lines as in the coasting beam theory /2-3 /. However these are based on the single-mode approximation and may not work well for the weakly unstable case when the turbulence sets in early before saturation.

5 Acknowledgements

I would like to acknowledge many usefull discussions with Pat Colestock. His advice and encouragement were essential.

References.

1. E.Keil, E.Meserschmid. Nucl.Instr. and Meth. 128 (1975) 203.

2. Y.Chin, K.Yokoya. Phys.Rev.D28 (1983) 2141.

3. S.Bogacz, K-Y Ng. Phys.Rev.D36 (1987) 1538.

4. R.H.Siemann. Nucl.Instr.Meth 221 (1984) 293.

5. C.Pelligrini. Proc. of 1981 US School on High En. Part. Accel.

6. T.Stix, The theory of plasma waves, McGraw-Hill,1993.

7. A.Gerasimov. Emittance growth at longitudinal bunched-beam instability: overshoot theory (to appear).

8. A.Chao, in *Physics of High En.Accel.*, Proc. of the Second Annual U.S. Summer School on High En. Part. Accel., Stanford, 1982, ed.M.Month, AIP Conf.Proc. No. 105, 1983.

9. F.Sacherer, A longitudinal stability criterion for bunched-beam instabilities, CERN/MPS/BR, 73-1 (1973).

APPENDIX A

The general expression for the collective force in the time domain is (see, e.g. /8/):

$$F(x,t) = \kappa \sum_{l=0}^{\infty} \int dx' \rho(x', t - lT_0) W(lL_0 + x' - x) \qquad \text{(A1)}$$

where $\rho(x,t)$ is the line density of the beam, $W(x)$ is the wakefield, T_0 is the revolution period, L_0 is the circumference of the ring and the summation is over all preceding revolutions. The intensity parameter κ is $\kappa = e\frac{\omega_0 I_0}{E_0}$ (with e for electron charge, I_0 for the bunch current and E_0 for the particle energy) /5/. The form (A1) is equivalent to a more familiar frequency-domain representation when the line density perturbation ρ' is a harmonic

function of time:

$$F'(x,t) = -i\kappa \sum_p \rho'_p Z(p+\Omega) e^{i(px-\Omega t)} \tag{A2}$$

where ρ'_p are the Fourier harmonics $\rho'(x,t) = \sum_p \rho'_p e^{i(px-\Omega t)}$, and $Z(\omega)$ is the impedance $Z(\omega) = \int dx e^{i\omega x \frac{T_0}{L_0}} W(x)$. The condition of the long wavelength of the wakefield relative to the bunch length is used in expanding the wakefield W in formula (A1) up to linear terms in the small argument $x' - x$. This yields the force as the sum $F = F_0 + F'$ of an incoherent (ρ-independent) part F_0 and a coherent part F'. The latter is found to be

$$F' = \kappa \sum_{l=0}^{\infty} \bar{x}(t - lT_0) W'(lL_0) \tag{A3}$$

where $\bar{x}(t) = \int dx' x' \rho(x',t)$ is the centoid coordinate and $W' = \frac{dW}{dx}$ is the wakefield derivative.

In our model (1), where the wakefield is localized (the interaction is δ-functional) the collective force $F = \sqrt{\epsilon/N} q \delta_{2\pi}$ can be expressed as

$$F(t) = \epsilon \delta_{2\pi} \sum_{n=0}^{\infty} \bar{x}\left([t]_{2\pi} - 2\pi n\right) W'(t - [t]_{2\pi} - 2\pi n) \tag{A4}$$

where $[t]_{2\pi}$ is the moment of time of the last "kick" $[t]_{2\pi} = 2\pi[t/2\pi]$ ([...] denotes the integer part). The quantity W' is given by

$$W'(t) = \sin(\omega_r t) e^{\omega_i t} \tag{A5}$$

where $\omega_r + i\omega_i = -i\alpha/2 + \sqrt{-\alpha^2/4 + \omega_c^2}$. This expression becomes equivalent to the distributed-wake (A2) if one utilizes the condition of the synchrotron frequency being much smaller then the revolution frequency $\omega_s \ll 1$. Indeed, averaging $F(t)$ over the "fast" time scale $\Delta t = 2\pi$ yields:

$$\bar{F}(t) = \frac{\epsilon}{2\pi} \sum_{n=0}^{\infty} \bar{x}([t]_{2\pi} - 2\pi n) W'(2\pi n) \tag{A6}$$

This is equivalent to the expression (A2) (with a specific choice of W' (A5) and $\kappa = \epsilon/2\pi$) since $\bar{x}(t)$ changes very little over the revolution period $\Delta t = 2\pi$.

APPENDIX B

Consider a multi-bunch longitidinal motion with a localized impedance of a long wavelength:

$$\ddot{x}_i^{(n)} + \omega_s^2 x_i^{(n)} - \lambda \left(x_i^{(n)}\right)^3 = \sqrt{\frac{\epsilon}{N}} q \delta_{2\pi}(t + 2\pi \frac{n}{M}) \qquad \text{(B1)}$$

$$\ddot{q}_l + \alpha_l \dot{q}_l + \omega_{cl}^2 q_l = \sqrt{N} \sum_{n=1}^{M} \sqrt{\epsilon_l} \bar{x}^{(n)} \delta_{2\pi}(t + 2\pi \frac{n}{M})$$

where $q = \sum_l \sqrt{\epsilon_l/\epsilon} q_l$ is the sum over different modes q_l with different frequencies ω_{cl} and damping decrements α_l that are coupled to the beam with a different coupling strength ϵ_l. Furthermore, M is the number of bunches and $x_i^{(n)}$ is the coordinate of the i-th particle in the n-th bunch. The representation of the wakefield in (B1) is fairly general as one can represent an arbitrary spectrum of impedance as a superposition of Lorentzian curves.

We assume now that the dominant modes of the wakefield are tuned near only one of the coupled-bunch mode frequencies $|\omega_c - (\mu + kM)| \ll 1$ (here μ is the coupled-bunch integer index between 1 and M) and that the width of the impedance peak near that coupled-bunch frequency is small $\Delta\omega_z \ll 1$ (right-hand side of condition *(i)*). These conditions allow us to have a single coupled-bunch mode dominating the dynamics.

As a next step, we assume that the interaction is weak $\epsilon \ll \alpha_l \omega_s^2 \omega_{cl}$ (condition *(ii)*) and the tune spread is small $\lambda\langle x^2 \rangle \ll \omega_s^2$. The first condition is necessary for the introduction of an effective impedance. The centroid oscillations $\bar{x}^{(n)}(t)$ then can be separated into the fast synchrotron oscillations with the frequency ω_s and a slowly changing envelope:

$$\bar{x}^{(n)} = a \cos(\omega_s t + 2\pi \frac{n\mu}{M} + \varphi) \qquad \text{(B2)}$$

where the amplitude a and the phase φ are slow functions of time. Expanding the periodic δ-function in Fourier series, one finds the dominant response of the cavity at positive and negative synchrotron sidebands of the resonant coupled-bunch frequency:

$$q = \frac{\sqrt{N}}{2\pi} \sum_l \sqrt{\frac{\epsilon_l}{\epsilon}} Re \left[\frac{a\, e^{i((\omega_s+\mu+kM)t+\varphi)}}{\omega_{cl}^2 - (\omega_s+\mu+kM)^2 + i\alpha_l(\omega_s+\mu+kM)} \right. \qquad \text{(B3)}$$

$$\left. + \frac{a\, e^{i((\omega_s-\mu-kM)t+\varphi)}}{\omega_{cl}^2 - (\omega_s-\mu-kM)^2 + i\alpha_l(\omega_s-\mu-kM)} \right]$$

In the first equation (B1), the two-time scale approximation allows us to retain only the Fourier component of the collective force $F = \sqrt{\epsilon/N} q \delta_{2\pi}(t + 2\pi\frac{n}{M})$ at the frequency ω_s, yielding:

$$\ddot{x}_i^{(n)} + \omega_s^2 x_i^{(n)} - \lambda \left(x_i^{(n)}\right)^3 = \epsilon Re \left[i\tilde{Z} a e^{i(\omega_s t + \varphi + 2\pi\frac{n}{M})}\right] \qquad \text{(B4)}$$

where $\tilde{Z}$ is the effective impedance $\tilde{Z} = Z(\omega_s)$. The impedance $Z(\omega)$ is:

$$\begin{aligned} Z(\omega) &= -\sum_l \frac{i\sqrt{\epsilon_l/\epsilon}}{(2\pi)^2} \left[\frac{1}{\omega_{cl}^2 - (\omega + \mu + kM)^2 + i\alpha_l(\omega + \mu + kM)}\right. \qquad \text{(B5)} \\ &\quad \left. + \frac{1}{\omega_{cl}^2 - (\omega - \mu - kM)^2 + i\alpha_l(\omega - \mu - kM)}\right] \end{aligned}$$

One can now extract the equation for the slowly varying quantities a and φ directly from equation (B4). Using the alternative slow variables for the centroid $\bar{y} = a\cos\varphi$, $\dot{\bar{y}} = -a\omega_s \sin\varphi$, and for individual particles $\bar{y}_i = a_i \cos\varphi_i$, $\dot{\bar{y}}_i = -a_i\omega_s \sin\varphi_i$ one obtains after averaging over the fast oscillations:

$$\ddot{y}_i + \omega_s^2 y_i - \frac{3}{8}\lambda(y_i^2 + \dot{y}^2/\omega_s^2)^{3/2} = \epsilon(-\tilde{Z}_i \bar{y} + \frac{\tilde{Z}_r}{\omega_s}\dot{\bar{y}}) \qquad \text{(B6)}$$

Equivalently, one can return to the initial variables $x_i = x_i^{(0)}, \dot{x}_i = \dot{x}_i^{(0)}$ and present the averaged equations of motion in the form

$$\ddot{x}_i + \omega_s^2 x_i - \lambda x_i^3 = \epsilon(-\tilde{Z}_i \bar{x} + \frac{\tilde{Z}_r}{\omega_s}\dot{\bar{x}}) \qquad \text{(B7)}$$

In our single-bunch, single-mode wakefield model (1), the effective impedance $\tilde{Z}$ is defined by only one term in the sum in expression (B5). Since one can achive arbitrary values of $\tilde{Z}_r$ and $\tilde{Z}_i$ by adjusting ω_c and α, the single-bunch model is fully equivalent, under specified restrictions, to the multi-bunch system (B1).